## ARTICLE

Check for updates

# Enhanced dielectric constant and energy density in a BaTiO₃/polymer-matrix composite sponge

Gang Jian [1✉], Yong Jiao[1], Qingzhen Meng[1], Zhaoyu Wei[2], Jiaoxia Zhang[1], Chao Yan [1], Kyoung-Sik Moon[3] & Ching-Ping Wong[3✉]

Polymer-matrix dielectric composites are promising for use in electrostatic energy storage devices due to the ultra-fast charge–discharge speed and the long service life. Here we report a strategy for designing BaTiO₃ sponge polymer composites for energy storage. BaTiO₃ sponges with tunable porosities are prepared from polymethyl methacrylate micro-sphere arrays. Liquid epoxy completely fills the pores in a BaTiO₃ sponge during vacuum de-foaming, forming a solid composite. The resulting composites possess a maximum dielectric constant of $\varepsilon_r$~332 and $\varepsilon_r/\varepsilon_m$~85, compared to $\varepsilon_r$~38 in a sample filled with BaTiO₃ NPs, at 1 kHz. The composites also possess, at 100 kV cm$^{-1}$, a high discharge energy density of $U_d$~105 × 10$^{-3}$ J cm$^{-3}$ and $U_d/U_m$~51, and electric displacement of 3.2 μC cm$^{-2}$, compared with those utilizing traditional strategies at low electric fields. Finite element simulation reveals the enhanced energy density is due to a high local electric displacement in composites.

[1] School of Materials Science and Engineering, Jiangsu University of Science and Technology, 212003 Zhenjiang, China. [2] School of Oceaography, Shanghai Jiao Tong University, 200240 Shanghai, China. [3] School of Materials Science and Engineering, Georgia Institute of Technology, Atlanta 30332, USA. ✉email: gjian@just.edu.cn; cp.wong@mse.gatech.edu

With the emergence of a series of thorny problems such as global warming and gradual exhaustion of fossil fuels, the exploitation of renewable resources has become a global priority. Most new energies like the wind energy and the solar energy, etc. are heavily dependent on energy storage units because of their intermittent nature. Among all kinds of energy storage technologies, the most environmentally friendly and long-used electrostatic capacitor has actively pursued in recent years, which is broadly applied in various fields, like automotive industries, computer systems as well as electronic weapons[1–4]. With continuous efforts on miniaturization and lightweight of electronic products, the demand for dielectrics possessing high-energy densities and low losses is increasing.

The energy density ($U$) is described as $U = 1/2\varepsilon_0\varepsilon_r E_b^2$ for linear dielectrics[5], where $\varepsilon_0$, $\varepsilon_r$, and $E_b$ are the vacuum permittivity, the relative dielectric constant, and the breakdown strength, respectively. As for nonlinear dielectrics whose dielectric constant changes with the electric field, the energy density is obtained from $U = \int E dD$[6,7], where $E$ is the electric field and $D$ is the electric displacement. Obviously, dielectric constant and breakdown strength are both vital in achieving high-energy densitites. Ceramics possess high dielectric constant, but their breakdown strengths are limited, while the corresponding properties of polymers are just the opposite[8]. According to previous studies, polymer–matrix composites containing ceramic fillers have better properties than single components, dielectric constants of polymer/ceramic composites could be enhanced by raising the loading level of ceramic fillers, and the breakdown strengths are maintained at high values[9].

However, the dielectric constant is still limited for polymer/ceramic composites compared with ceramics. As for traditional polymer/ceramic nanoparticles (NPs) composites, dielectric constant at 1 kHz of most reported studies is below 50. Surface modications of ceramic NPs improve the compatability between organic and inorganic phases but plays a minor part in raising dielectric constants[2,7]. By using one-dimensional ceramic structures, i.e., nanowires (NWs) and nanofibers of BaTiO$_3$ (BT)[10], Pb(Zr,Ti)O$_3$ (PZT)[11], ZnO[12], NaNbO$_3$, etc.[13], considerably improved (~15% to ~50% of enhancement) dielectric constant and energy density compared with polymer/ceramic NPs composites are achieved. Vertical alignments of ceramic NWs in composites show further enhancements in dielectric performances[14,15]. Besides to one-dimensional composites, a study by Luo et al.[16] of a polymer composite filled with a lignocellulose template-based ceramic network shows a dielectric constant of 200 (1 kHz) and a discharged energy density ($U_d$) of $12.8 \times 10^{-3}$ J cm$^{-3}$ at 100 kV cm$^{-1}$.

It is found that the tailoring of filler architecture is an approach to the enhanced dielectric constant of composites, however, issues still exist. Fistly, it is challenging to obtain three-dimensional

ceramics with increased performances in composites because of difficulties in simultaneously achieving the high microscopic uniformity and the macroscopic free-standing[17–20]. For instance, a relatively high loss of ~0.14 at 1 kHz is obtained in Luo et al.'s work[16] at a filler loading of 30 vol%, which may be due to the method using lignocellulose templates is difficult to control the microstructure details of the network. Secondly, traditional effective medium theory (EMT) for composites also considers filler morphology's effect on dielectric constants with an fitting factor, however, it cannot provide a specific filler achitecture as it predicts to have high dielectric constants[21]. A relation between the fitting factor and the specific morphology is required to be built. At last, as for nanowire-based composites, studies show that enhanced electric displacement is arising from the high adjacent polarizations around NWs[13], while the mechanism of enhanced electric displacement in interconnected filler-based composites is not clearly understood yet. Therefore, to design novel filler achitectures and composites with further enhanced performances and investigate inherent mechanisms in interconnected filler-based composites will be of great significance.

In this work, well-designed BT sponge structures are initially prepared from polymethyl methacrylate (PMMA) micro-sphere arrays, which filler architecture exhibits precisely tunable porosity and high uniformity. The epoxy/BT sponge composites are prepared by mixed by vacuum de-foaming method and capillary force and then cured. By comparing various dielectric models, the shape fitting factor in the EMT model corresponding to BT sponges is determined to be 0.01. Finite-element simulation as well as the surface potential and charge density distribution analyses show that the high local electric displacement is the main reason for enhanced energy densities. Epoxy/BT sponge composites possess $\varepsilon_r$ ~ 332 (1 kHz) and $U_d$ ~ $105 \times 10^{-3}$ J cm$^{-3}$ (at 100 kV cm$^{-1}$). Results show that the epoxy/BT sponge composite with good dielectric and energy storage characteristics have very promising electrostatic capacitors for energy storage.

## Results and discussion

**Prepration and the BT sponge and epoxy/BT composites.** Three-dimensional BT sponge structures with various porosities are critical to obtain epoxy/BT composites with tunable filler loadings. The fabrication schematic of three-dimensional BT sponge structures and corresponding composites is shown in Fig. 1. To fabricate a BT sponge, PMMA microspheres are employed to generate pores in solid BT bodies after the decomposition of the spheres where volume fraction of the sphere may determine the porosity of the sponge; a sintering process is then conducted to form a free-standing BT structure rather than being collapsed into discrete powders. And then the external vacuum de-foaming is conducted to discharge air bubbles inside the epoxy-immersed BT sponge, thus to improve wetting of the liquid epoxy on the inner and outer surfaces of the porous sponge, prior to the curing process (Supplementary Methods, Supplementary Fig. 1). Also, the porosity of the BT sponge has to be in a suitable range so that an acceptable mechanical property of composite can be made from it. It is found that the high porosity over 80% makes the sponge fragile and hard to hold by hands, while the low porosity <50% renders mostly closed pores and inside ones would remain empty without epoxy filling.

Figure 2a, b show the Fourier transform infrared (FTIR) spectrum and the scanning electron microscopy (SEM) image of PMMA microspheres utilized as templates for generating pores in BT structures. The PMMA molecular structure is confirmed by the FTIR spectrum[22] (Fig. 2a) and uniform spherical shapes of PMMA particles with a mean diameter of ~50 μm (the inset of Fig. 2b) are observed from the SEM image (Fig. 2b). Figure 2c, d
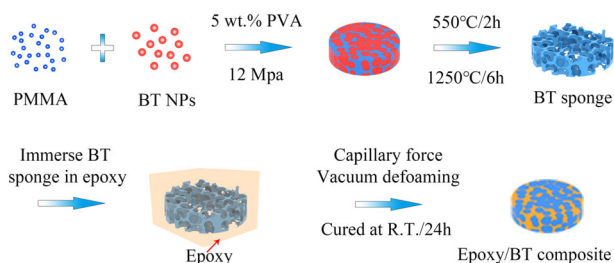


**Fig. 1 Schematic illustration of the preparation of the ceramic filler and the composite.** The preparation of sponge-like BT three-dimensional structures by using PMMA-sphere arrays as templates. The preparation of epoxy/BT sponge composites by the capillary force and the vacuum defoaming.
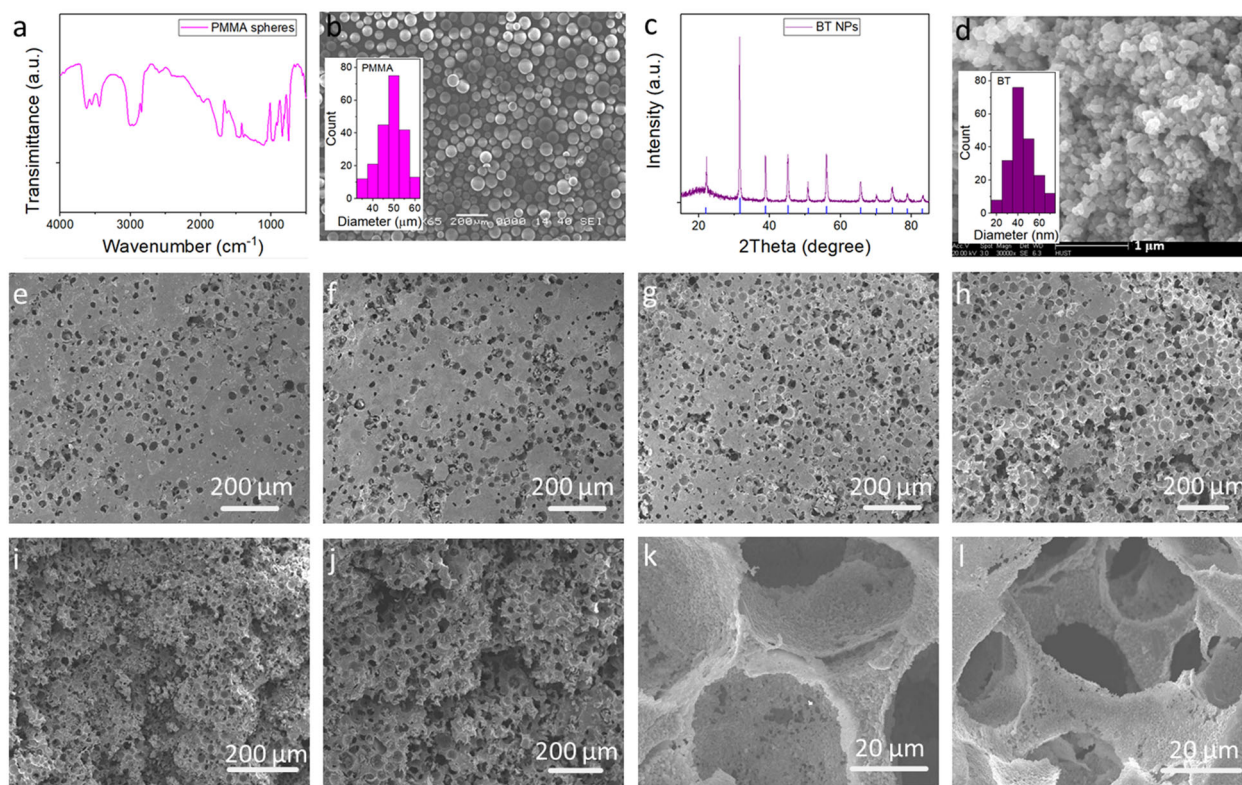
**Fig. 2 Characterization of density tunable BT sponges. a, b** FTIR spectrum and SEM image of PMMA microspheres. **c, d** XRD pattern and SEM image of synthesized BT NPs from the sol–gel method. Insets of **b** and **d** are diameter distributions of PMMA spheres and BT NPs, respectively. **e–h** Surface SEM images of BT sponges with different porosity: **e** 50%, **f** 60%, **g** 70%, and **h** 80%. **i, j** Cross-sectional SEM images of BT sponges. **k, l** Detail cross-sectional SEM morphology images of BT sponges.

show the X-ray diffraction (XRD) pattern and the SEM image of synthesized BT NPs by sol–gel method which is also a raw material to prepare the BT sponge. The BT particles are also of the uniform shape (Fig. 2d) with a mean size of ~40 nm (the inset of Fig. 2d), and the diffraction pattern's corresponding JCPDS No. 31-0174 indicates a cubic phase of BT ($a = 0.4031$ nm[23,24], Fig. 2c).

Figure 2e–h show the SEM images of BT sponges with the porosity of 50%, 60%, 70%, and 80% after calcined at 450 °C for 2 h and sintered at 1250 °C for 6 h (see Supplementary Note 1, Supplementary Figs. 2 and 3). On the surface of samples, pores can be evidently observed with consistent diameters, about 50 μm, corresponding to the size of PMMA spheres. These pores are not only evenly distributed on the surface, but also can be seen from the cross-sectional SEM images of sponge structures in Fig. 2i, j. In BT sponges, the pores are uniformly distributed and interconnected within the materials, which provides a condition for the irrigation of polymers to prepare composite materials. Also, the BT frameworks give a macroscopic free-standing sponge structure which is actually obtained through heat treatment[25]. The magnified SEM images in Fig. 2k, l further indicate that the pores are interconnected and the BT wall thickness is in the range of micron meters. To further confirm the BT sponge structures, samples have gone through water-drops permeation tests. It can be found that all samples with the porosity ranging from 50% to 80% can permeate water-drops completely, which indicates pores inside the material are interconnected and the fabrication of composites from the BT sponge is reasonable. With increasing the porosity, the permeation rate of water-drop is faster (0.5–2 s per drop for porosity 80–50%), which is due to the higher amount of pores inside the bodies.

Figure 3a–d show the cross-sectional SEM images of epoxy/BT sponge composites. It can be found that the epoxy matrix and the BT can be clearly distinct in the composites. The BT shows an annularly interconnected network in the epoxy matrix, which is due to the fillers' sponge shape. And it can be deduced that BT has a regular three-dimensional filling fashion in the epoxy matrix. From the detailed SEM images in Fig. 3c, d, good contacts between the BT structure and the epoxy matrix without evident cracks and pores are observed, which indicates that liquid epoxy has filled completely the interspace of BT sponges. The BT is also confirmed by energy-dispersive X-ray (EDX) mappings, with results shown in Fig. 3e, f. Distribution mappings of Ba (L-edge) and Ti (k-edge) are almost identical, which shape and position are in accordance with the BT morphology in Fig. 3d.

Figure 4a shows FTIR spectra of epoxy/BT sponge composites at various filler loadings. It is well known that the characteristic vibration peak of uncured epoxy occurs at 913.25 cm$^{-1}$ [26]. It is clearly observed that characteristic peaks of the neat epoxy and composites disappear at 913.25 cm$^{-1}$, which can be explained that materials have been completely cured. Also, the epoxy resin phase can be confirmed from the typical peaks at 1032 cm$^{-1}$ (C–O) and 1507 cm$^{-1}$ (C–C), etc.[27]. Vibration peaks of the neat epoxy can be also observed in FTIR spectra of epoxy/BT sponge composites, indicating the containing of the epoxy. The vibration at 1626 cm$^{-1}$ is due to the BT loading in composites[28]. Supplementary Fig. 4 shows XRD patterns of epoxy/BT sponge composites, from which the epoxy and BT can be confirmed, respectivley, also see Supplementary Note 2.

According to the thermogravimetric analysis (TGA) diagram of epoxy/BT sponge composites and a neat epoxy (Fig. 4b), the decomposition temperature of epoxy is ~410 °C[29]. TG curves are
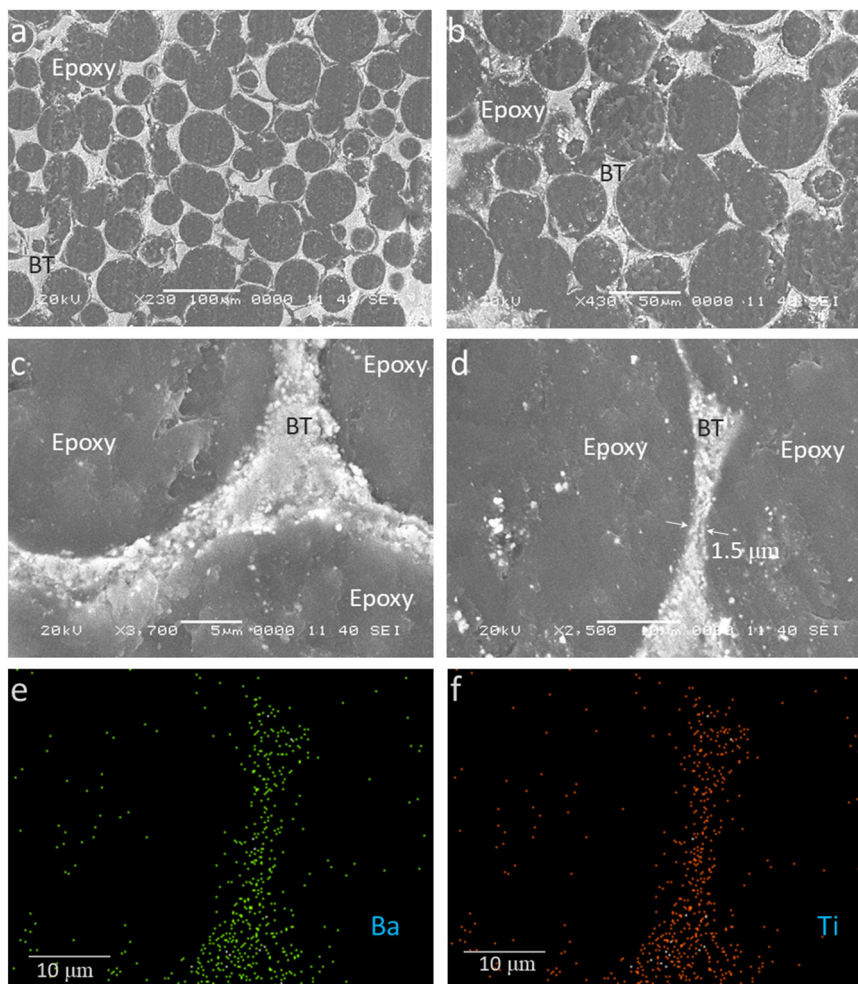
**Fig. 3 Microstructural morphology and composition of epoxy/BT sponge composites. a–d** Cross-sectional SEM images of epoxy/BT sponge composites. The white and gray colors correspond to BT and epoxy resin, respectively. **e, f** EDX mappings of Ba (L-edge) and Ti (K-edge) distributions corresponding to **d**.

divided into two stages. At the first stage (100–300 °C), the water adsorbed on the surface is removed, so the weight decline is relatively gentle. The second stage (300–450 °C) is the decomposition stage of epoxy resin, which is completely decomposed at about 450 °C[30]. The weight analysis indicates the reduced weight is corresponding to the weight decrease of the epoxy resin. The weight change is ~92 wt% for the neat epoxy, left with a residual ~8 wt%. TG curves "1–4" correspond to epoxy/BT sponge composites at various filler loadings, the weight loss at 450 °C are ~7, ~13, ~22 and ~33 wt%, respectively. Based on the theoretical density of 6.02 g cm$^{-3}$ of BT[31] and the measured density of 1.06 g cm$^{-3}$ of the epoxy, the volume fraction of BT can be calculated to be ~50, ~40, ~30 and ~20 vol%, respectively, The TG tests show that the filler loadings of the composite are properly prepared as close as designed which further confirms the complete permeation of the liquid epoxy into the interspace in BT sponges.

Figure 4c shows the stress versus strain behavior of epoxy/BT sponge composites and the neat epoxy, from which mechanical properties can be obtained. By filling the BT sponge, epoxy composites possess increased modulus. At the 1% strain, the modulus of epoxy/BT sponge composites with $f_{BT}$ (vol) of 0%, 20%, 30%, 40%, and 50% is 2800, 4900, 5800, 7300, and 9600 MPa, respectively. The tensile strength also increases from 90 MPa (the epoxy) to 175 MPa (the epoxy/50% BT sponge composite) while the strain has a contrary fashion, decreasing

from 5.1% (the epoxy) to 2.3% (the epoxy/50% BT sponge composite). The filling of rigid BT with high modulus into epoxy with lower modulus is the main contribution to the mechanical-properties adjustment[32,33]. At the same time, the BT sponge architecture in the epoxy is almost unchanging except for the thickness at various filler loadings, which results a continuous changing of mechanical properties of composites.

**Dielectric characteristics of composites.** Figure 5a, b show frequency-dependent dielectric properties of BT/epoxy composites at room temperature. The dielectric constants of epoxy/BT composites are much increased compared with that of the neat epoxy at the whole frequency range investigated; with increasing $f_{BT}$ (vol) in composites (20–50%), increased dielectric constants are achieved. The dielectric constants in epoxy/BT sponge composites at $f_{BT}$ (vol) of 0%, 20%, 30%, 40%, and 50% at 10 Hz are 3.9, 98, 163, 285, and 436, respectively. Epoxy/BT composites exhibit a slightly decreasing fashion in the frequency dependence of dielectric constants, which is due to a typical nature of Maxwell–Wagner–Sillars (MWS) polarization[34]. MWS polarization is generated in organic/inorganic interfaces in composites due to the difference in dielectric constants, which cannot catch up with the alternating high frequencies, resulting decreased dielectric constants with the frequency. The similar fashion is also obtained in the dielectric loss (tanδ) in Fig. 5b. Figure 5b also
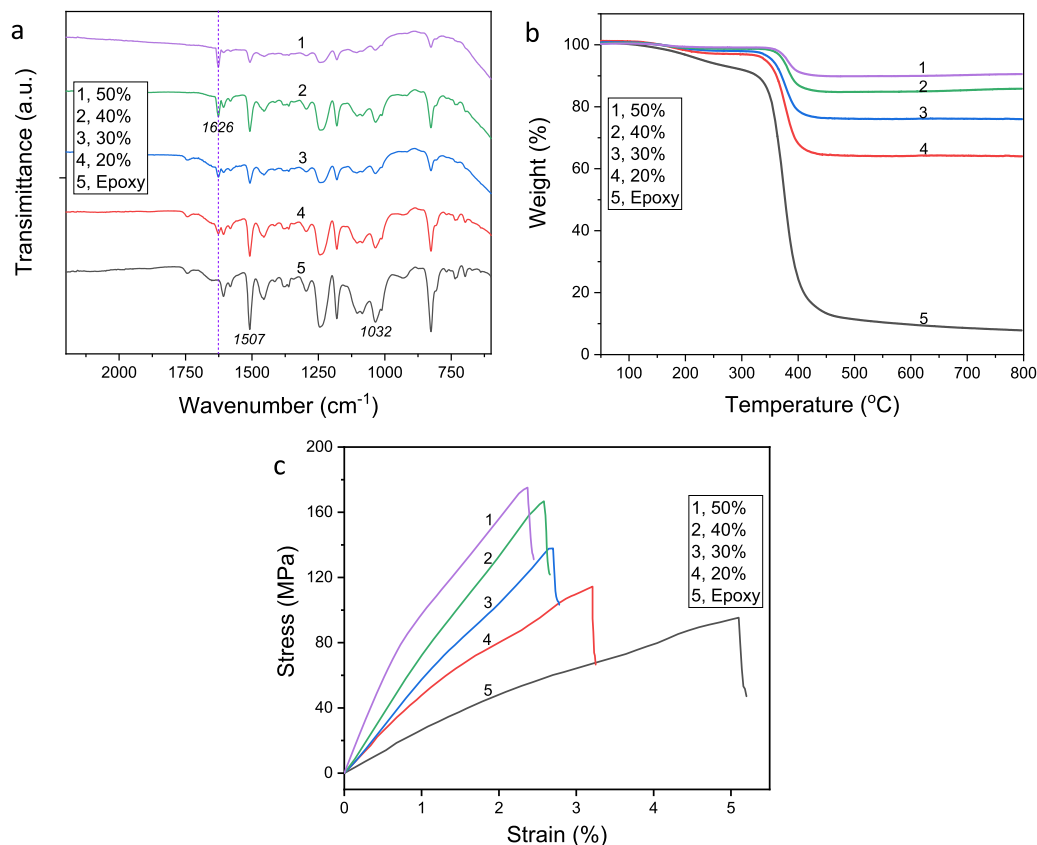
**Fig. 4 Compositional, thermal, and mechanical properties of epoxy/BT sponge composites. a** FTIR of epoxy/BT sponge composites with various BT loadings. **b** TGA patterns in air of epoxy/BT sponge composites with various BT loadings. **c** Stress versus strain behaviour of epoxy/BT sponge composites with various BT loadings.

shows that the epoxy/BT sponge composites exhibit a low tanδ (<0.03), at a same level with that of the neat epoxy, indicating the material could be well served as dielectrics for capacitors[6,26]. The low-dielectric loss is due to the good compatability between BT sponges and the epoxy matrix. The dielectric constant imaginary part ($\varepsilon''$) is the product of tanδ and the dielectric constant real part, which describes energy dissipations in dielectrics via the conduction, slow polarization currents or other dissipative phenomena-like interfacial polarizations[35]. The inset of Fig. 5b shows frequency-dependent $\varepsilon''$ of the epoxy/BT sponge composites and the neat epoxy. A first decreasing and then stable fashion can be observed, similar to results for epoxy/BT composites in the literature[35], which indicates that conduction and interfacial polarization loss occur at low frequencies, while frequency-dependent changings are small for the loss and relaxation contributions at high frequencies such as 1 kHz.

In order to reveal filler shape effects on composites' dielectric properties, epoxy/BT NPs, and epoxy/BT NWs composites (SEM images are shown in Supplementary Fig. 5) are investigated to compare with the epoxy/BT sponge composites. In Fig. 5c, the dielectric constants at 1 kHz in epoxy/BT sponge composites are much higher compared with that of epoxy/BT NPs and epoxy/BT NWs composites at all filler loadings investigated. At $f_{BT}$ of 50%, the dielectric constant at 1 kHz is 332 for epoxy/BT sponge composites, while the values are 50.3 and 38 for epoxy/BT NWs and epoxy/BT NPs composites, respectively. Various theoretical models on prediction of effect dielectric constants at a constant frequency of composites have been proposed to compare with experiment results and to understand dielectric behavior mechanisms in composites. Theoretical predictions include the parallel mixing model[36,37], the series mixing model[36,37], the

logarithmic mixing model[38] and the EMT model[21]. The different models are expressed as

$$\text{Parallel mixing model}: \ \varepsilon_r = (1-f)\varepsilon_m + f\varepsilon_f, \qquad (1)$$

$$\text{Series mixing model}: \frac{1}{\varepsilon_r} = \frac{1-f}{\varepsilon_m} + \frac{f}{\varepsilon_f}, \qquad (2)$$

$$\text{Logarithmic mixing model}: \ \log \varepsilon_r = (1-f)\log \varepsilon_m + f \log \varepsilon_f, \qquad (3)$$

$$\text{EMT}: \ \varepsilon_r = \varepsilon_m \left(1 + \frac{f(\varepsilon_f - \varepsilon_m)}{\varepsilon_m + n(1-f)(\varepsilon_f - \varepsilon_m)}\right). \qquad (4)$$

where $n$ is the fitting factor for the filler morphology, $f$ is the volumetric filler loading, $\varepsilon_r$, $\varepsilon_f$, and $\varepsilon_m$ are dielectric constant for the composite, the filler and the matrix, respectively.

Notably, although these models are mostly treated as prediction models for direct current (DC) dielectric constants, it is applicable to predications of the equivalent dielectric constant in epoxy/BT composites at 1 kHz in this study, due to that the filler loading is the main parameter influencing dielectric properties of epoxy/BT sponge composites in this frequency region. The stable tanδ and $\varepsilon''$ characteristics (Fig. 2b) at frequencies of 1 kHz and above indicate that there is no much frequency-dependent changing in interactions between constituents, relaxations, and interfacial poarizations in epoxy/BT sponge composites.

From the experimental and theoretical comparisons in Fig. 5c, dielectric constants of epoxy/BT sponge composites exceed the logarithmic model, while dielectric constants of epoxy/BT NWs and epoxy/BT NPs composites both fall in between the
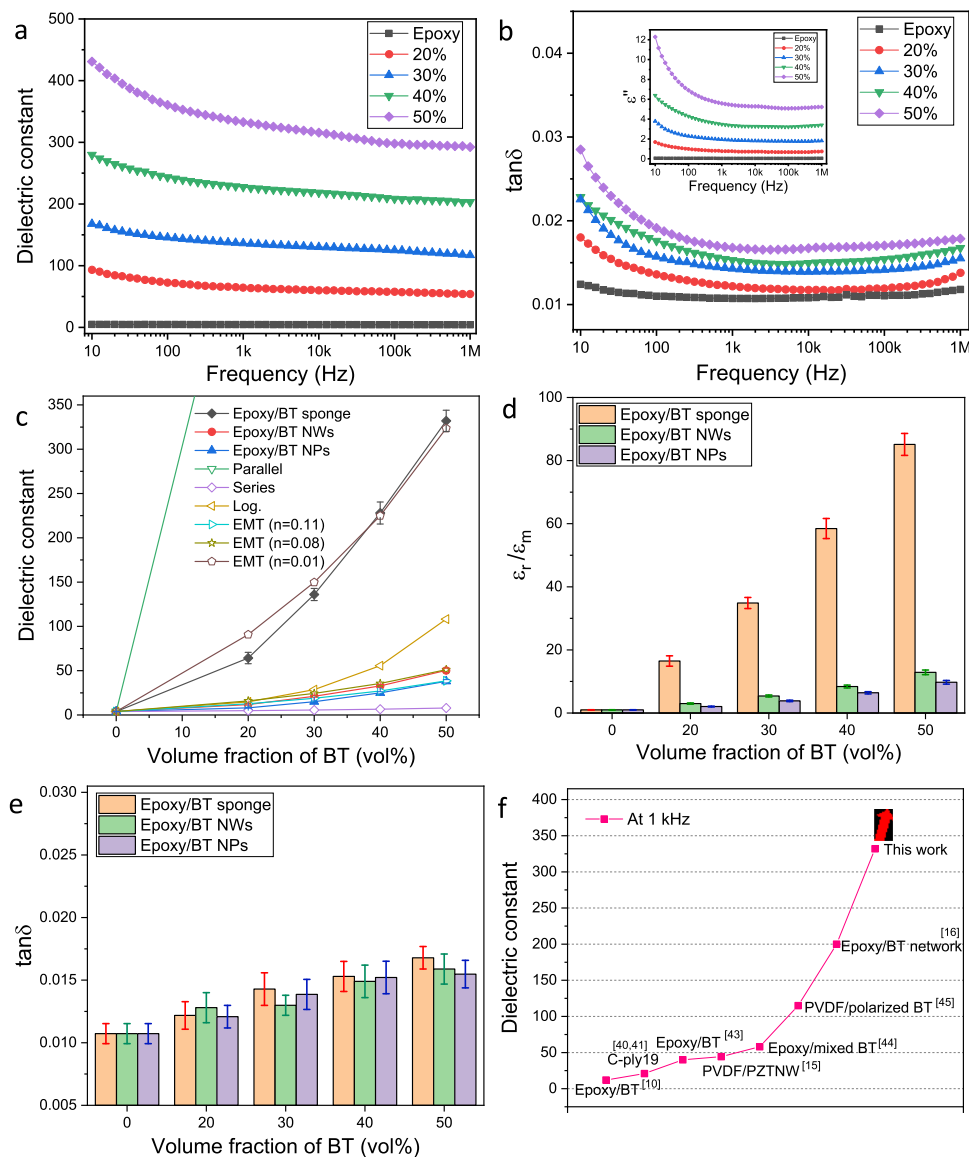
5

**Fig. 5 Dielectric characteristics of epoxy/BT sponge composites and counter parts filled with other BT fillers.** Frequency dependencies of **a** dielectric constant and **b** dielectric loss (tan$\delta$) of epoxy/BT sponge composites with various BT loadings at room temperature. The inset of **b** is frequency-dependent imaginary part ($\varepsilon''$) of dielectric constant of epoxy/BT sponge composites with various BT loadings at room temperature. **c** Dielectric constants at 1 kHz of epoxy/BT composites with various shapes and various theoretical prediction models. **d** Enhancement of dielectric constant ($\varepsilon_r/\varepsilon_m$) and **e** tan$\delta$ at 1 kHz in composites of epoxy/BT sponge, epoxy/BT NWs, and epoxy/BT NPs. **f** Comparison of dielectric constant in polymer-composites in our work and in literatures. Error bars are SEM.

logarithmic model and the series model. It also indicates that dielectric constants of epoxy/BT sponge composites have fallen in the missing area in the $\varepsilon_r \sim f$ plot[16,39], which is not achieved by the filling of BT NWs and BT NPs. $n$ in the EMT model is a factor reflecting influences of filler shapes. Based on the dielectric constant of BT ($\varepsilon_r \sim 3000$) and the epoxy resin ($\varepsilon_r \sim 3.9$), the dielectric constants of epoxy/BT NPs and epoxy/BT NWs composites fit the EMT model with $n = 0.11$ and $n = 0.08$, respectively, which are typical fitting values for spherical and wire-shaped fillers[21,39]. For epoxy/BT sponge composites, the dielectric constant is consistent with the EMT model with a much decreased fitting factor of $n = 0.01$. Decreased $n$ in the EMT model means increased spatial continuity of the filler, therefore, the enhanced dielectric constant in epoxy/BT sponge composites can be explained by the constructed high spatial continuity of the filler in composites.

The dielectric constant enhancement ($\varepsilon_r/\varepsilon_m$) is also a parameter reflecting the filler's improvement degree of dielectric constants from the polymer. Figure 5d presents the comparison of $\varepsilon_r/\varepsilon_m$ among epoxy composites filled with various types of BT. It can be found that $\varepsilon_r/\varepsilon_m$ for the epoxy/BT sponge ($\varepsilon_r/\varepsilon_m \sim$ 16.4–85) is much higher than the epoxy/BT NWs ($\varepsilon_r/\varepsilon_m \sim$ 3–12.9) and the epoxy/BT NPs ($\varepsilon_r/\varepsilon_m \sim 2.1$–9.7) at $f_{BT} \sim 20$–50%. To our best knowledge, $\varepsilon_r/\varepsilon_m \sim 85$ is also the highest than values of commercial materials (e.g., C-ply19, 3M Company)[40,41] and ever reported polymer/ceramic dielectric composites[42–45]. Besides to the high permittivity in the BT itself ($\varepsilon_r \sim 3000$)[46], the unique architecture of the BT filler is a primary contribution. The dielectric loss for epoxy/BT sponge composite is slightly higher than that of epoxy/BT NPs and epoxy/BT NWs composites, but still at a low level (0.013–0.02), as shown in Fig. 5e, f summaries the dielectric constant of various polymer
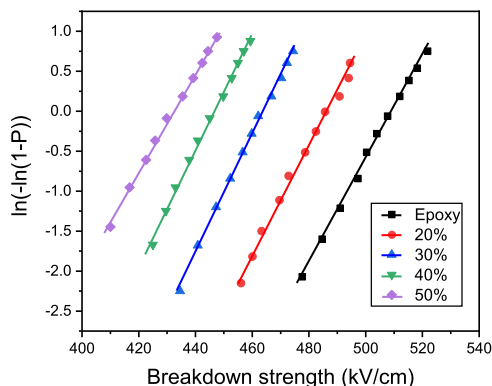
**Fig. 6 Breakdown strength characteristics of epoxy/BT sponge composites.** A Weibull distribution of the breakdown strength of epoxy/BT sponge composites with various BT loadings.

composites at 1 kHz reported in literatures. The dielectric constant in the epoxy/BT sponge composite of this study is higher than most polymer/ceramic composites made from traditional approaches, including the usage of NPs, NWs, polarized particles, and BT networks.

**Energy storage performances of composites.** Figure 6 shows the Weibull distribution plot of the breakdown strength of epoxy/BT sponge composites at various filler loadings. The statistical failure probability ($P$) is obtained in the form of $P = \exp[(E/E_0)^\beta][47]$ from test samples of at least 10 in each experiment, where $E_0$ is a scale parameter corresponding to $E_b$ at $P = 0.632$ (i.e., the value of $1 - 1/e \approx 0.632$) and $\beta$ is a shape parameter[47]. It is shown that $E_b$ values for epoxy/BT sponge with $f_{BT}$ of 0%, 20%, 30%, 40%, and 50% are 510, 485, 463, 446, and 432 kV cm$^{-1}$, respectively. The breakdown strength of composites decreases with the BT loading which is owing to the increase of inorganic–organic interfacial defects[48,49]. The breakdown strengths for epoxy/50% BT NWs and epoxy/50% BT NPs are 472 and 460 kV cm$^{-1}$, respectively, indicating similar level of breakdown strength is achived in epoxy/BT sponge composites compared with that of expoy composites filled with zero-dimensional or one-dimensional BT particles.

In order to obtain the energy storage performances, $D$–$E$ hysteresis loops of the epoxy/BT sponge composites with different filler loadings at various electric fields are studied (10 Hz). Figure 7a shows $D$–$E$ loops of epoxy/50% BT sponge composites at different electric fields. It can be found that all hysteresis loops exhibit a narrow shape, indicating a low loss of energy, i.e., the area within the loops. With increasing the electric field, the loop is getting flatter which may be due to the electrical resistivity nature at higher electric fields[14]. The electric displacement for epoxy/50% BT sponge composite at 20, 40, 60, 80, and 100 kV cm$^{-1}$ are 0.5, 1.1, 1.72, 2.3, and 3.2 µC cm$^{-2}$, respectively. Figure 7b shows $D$–$E$ loops of epoxy/BT sponge composites at various BT loadings at 100 kV cm$^{-1}$. When the filler loading increases from 0% to 50%, enlarged loops are observed indicating enhanced electric displacements. For comparison, $D$–$E$ loops of epoxy/50% BT NWs and epoxy/50% BT NPs composites at 100 kV cm$^{-1}$ are also provided, as presented in the inset of Fig. 7b. It can be found that the largest electric displacement is obtained in epoxy/BT sponge composites compared with other two types of BT composite fillers. At 100 kV cm$^{-1}$, the electric displacements for epoxy/BT sponge composites filled with $f_{BT}$ of 0%, 20%, 30%, 40%, and 50% are 0.04, 0.5, 1.1, 2.1, and 3.2 µC cm$^{-2}$, respectively (also see Supplementary Fig. 6); the electric displacements for epoxy/50% BT NWs and epoxy/50% BT NPs composites are 0.395 and 0.322 µC cm$^{-2}$, respectively. It is shown that the trend electric displacement is also in accordance

with the result of dielectric constant, i.e., a higher electric displacement results from a higher dielectric constant. From Fig. 7c, for epoxy/BT sponge composites with various filler loadings, electric displacements increase with increasing the electric field, attributing to the fact that more charges are generated under a higher electric field.

The charge energy density ($U_t$) and $U_d$ are calculated from the integration of $U = \int E dD$[6,7] adopting the right and the left curves of the $D$–$E$ loop, respectively, with results shown in Fig. 7d. $U_d$ increases continuously with electric field indicating that more energy is stored using a higher electric field; $U_d$ also increases with filler loadings of the BT sponge, which is owing to the enhanced dielectric constants and electric displacements. At 100 kV cm$^{-1}$, $U_d$ of epoxy/BT sponge composites with $f_{BT}$ of 0%, 20%, 30%, 40%, and 50% is $2 \times 10^{-3}$, $20 \times 10^{-3}$, $47 \times 10^{-3}$, $72 \times 10^{-3}$, and $105 \times 10^{-3}$ J cm$^{-3}$, respectively. The $U_d$ for epoxy/50% BT NWs and epoxy/50% BT NPs composites are $16 \times 10^{-3}$ and $13 \times 10^{-3}$ J cm$^{-3}$, respectively. It can be also found that $\varepsilon_r$ and $U_d$ can be tailored in this three-dimensional composite which is owing to the tunable porosity of the BT sponge. Figure 7e shows charge–discharge efficiency ($\eta = U_d/U_t \times 100\%$) of epoxy/BT sponge composites. Due to the high insulation and the low-dielectric loss of epoxy/BT sponge composites, high efficiency with low-energy loss is obtained during the energy storage. For epoxy/50% BT sponge composite, the efficiency is 63% at 100 kV cm$^{-1}$, in the same level of that of epoxy/50% BT NWs ($\eta \sim 62\%$) and epoxy/50% BT NPs ($\eta \sim 66\%$) composites.

The enhancement of energy density ($U_d/U_m$) is a reflection of filler's contribution on energy storage properties of composites. In Fig. 7f, compared with epoxy/50% BT NWs ($U_d/U_m \sim 8$) and epoxy/50% BT NPs ($U_d/U_m \sim 6.5$), the highest $U_d/U_m \sim 51$ is obtained in the epoxy/50% BT sponge composite. The energy density of the epoxy/50% BT sponge composite is also higher than reported values of $12.8 \times 10^{-3}$–$45.8 \times 10^{-3}$ J cm$^{-3}$ for polymer/ceramic composites at 100 kV cm$^{-1}$ [16,45,50–52]. The inset of Fig. 7f shows practical discharge characteristics of the epoxy/50% BT sponge composite capacitor. The capacitor (~2 µF, 1 kHz) is charged to 100 kV cm$^{-1}$ (1 kV is utilized for thickness ~100 µm) at first and then discharged through a 2 kΩ resistor. The voltage–time curve of the capacitor ($V_c$) takes a typical pulse-like shape[53], indicating potential applications in pulse power sources. The time constant of the circuit ($R_L C = 4$ ms) is in consistent with the milliseconds discharge time. The practical total discharged energy density is calculated to be $112 \times 10^{-3}$ J cm$^{-3}$ that is in consistent with $D$–$E$ results of $105 \times 10^{-3}$ J cm$^{-3}$. Notably, at 400 kV cm$^{-1}$, the epoxy/50% BT sponge composite possesses $D \sim 13.2$ µC cm$^{-2}$, $U_d \sim 1812 \times 10^{-3}$ J cm$^{-3}$ and $\eta \sim 58\%$ (see Supplementary Fig. 7). Table 1 summarizes dielectric and energy storage performances in this work and in literatures. Significant enhanced dielectric constants and energy densities are achieved in epoxy/BT sponge composites compared with those of composite counterparts made by traditional strategies.

**Local electric displacement enhancements.** In order to understand mechanisms of enhanced electric displacement and energy density in epoxy/BT sponge composites, the finite-element analysis (FEA) is conducted. Based on the dielectric constant (BT, 3000; the epoxy, 3.9) and the electrical conductivity (BT, 10$^{-9}$ S cm$^{-1}$; the epoxy, 10$^{-14}$ S cm$^{-1}$) of the materials, simulated electric displacements in composites of epoxy/BT sponge, epoxy/BT NWs, and epoxy/BT NPs are shown in Fig. 8a–c, respectively. Due to the heterogeneous nature of composites, voltages and electric displacements are not uniformly distributed inside composites (also see Supplementary Fig. 8). Notably, distinct differences in electric displacement are observed among composites
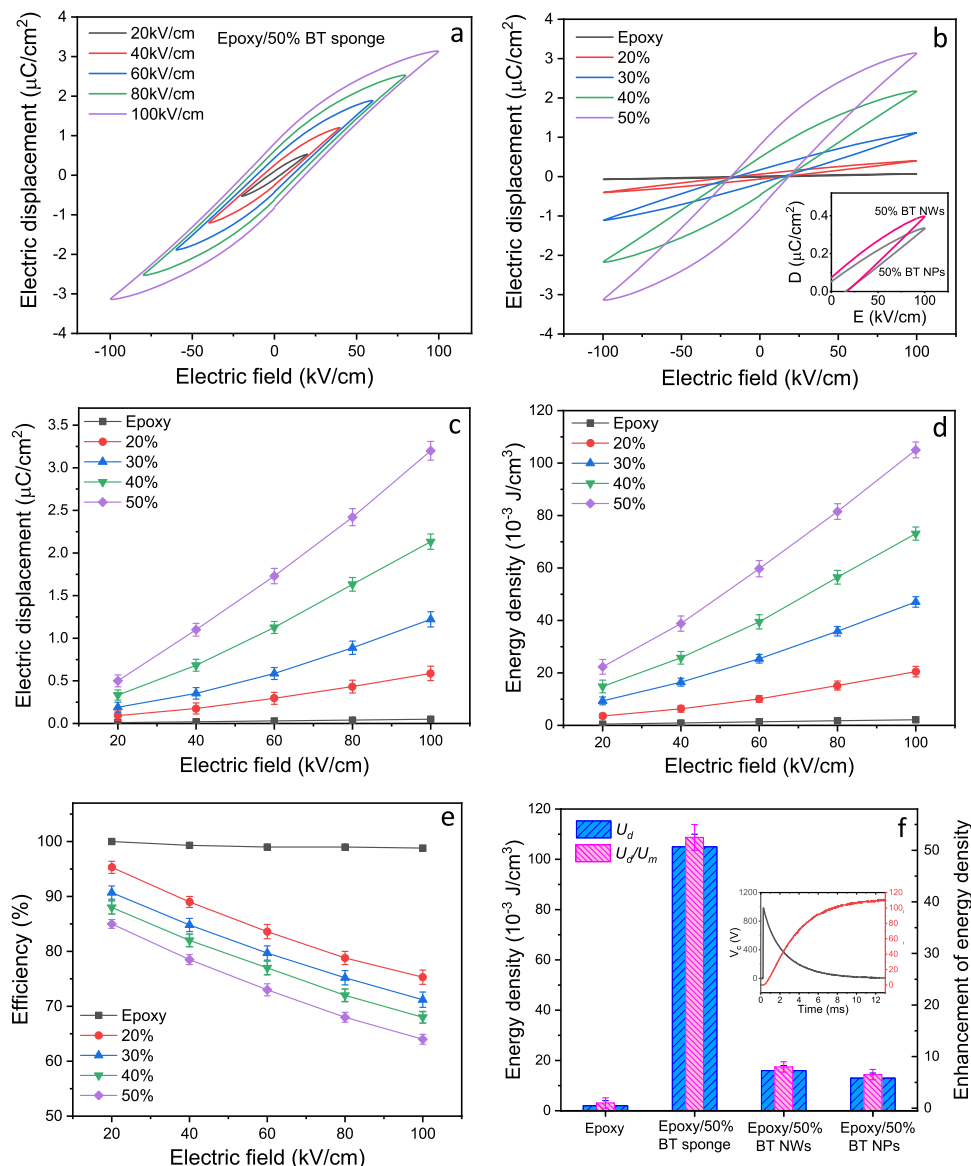
**Fig. 7 Energy storage performances of epoxy/BT sponge composites and conuterparts filled with other BT fillers. a** *D–E* loops at 10 Hz of epoxy/50% BT sponge composites at various electric fields. **b** *D–E* loops at 10 Hz of the neat epoxy and epoxy/BT sponge composites with various BT loadings. The inset of **b** is *D–E* loops at 10 Hz for epoxy/50% BT NWs and epoxy/50% BT NPs composites. **c** Electric displacement, **d** discharged energy density, and **e** charge–discharge efficiency of the epoxy and epoxy/BT sponge composites at various electric fields. **f** Comparison of enhancement of discharged energy density ($U_d/U_m$) at 100 kV cm$^{-1}$ of epoxy composites filled with the 50% of BT sponge, BT NWs, and BT NPs. The inset of **f** is the voltage ($V_c$) on the epoxy/50% BT sponge composite capacitor and discharged energy density ($U_d$) of the epoxy/50% BT sponge composite capacitor upon charged to 100 kV cm$^{-1}$ in the practical discharge curve test (the capacitance is ~2 μF; the load in series is 2 kΩ). Error bars are SEM.

**Table 1 Comparison of dielectric at 1 kHz and energy storage properties at 100 kV cm$^{-1}$ in our work and references.**

| Material | $f_{BT}$ (vol%) | $\varepsilon_r$ | $\varepsilon_r/\varepsilon_m$ | tan$\delta$ | $E_b$ (kV cm$^{-1}$) | $U_d$ (10$^{-3}$ J cm$^{-3}$) | $U_d/U_m$ | Ref. |
|---|---|---|---|---|---|---|---|---|
| Polyvinylidene fluoride/PZT NWs | 40 | 45 | 4.5 | | | 22 | | [15] |
| Epoxy/BT NPs | 50 | 40 | 10.5 | | | | | [43] |
| Epoxy/BT network | 30 | 200 | 55.4 | 0.14 | 265 | 12.8 | 25.6 | [16] |
| 3M C-ply19 | 40 | 21 | | 0.03 | 1300 | | | [40,41] |
| Polyvinylidene fluoride/BT NPs | 60 | 115 | 11.5 | 0.02 | | 45.8 | | [45] |
| Epoxy/BT NWs | 50 | 50.3 | 12.9 | 0.016 | 472 | 16 | 8 | Our work |
| Epoxy/BT NPs | 50 | 38 | 9.7 | 0.015 | 460 | 13 | 6.5 | |
| Epoxy/BT sponge | 20 | 64 | 16.4 | 0.013 | 485 | 20 | 10 | |
| | 30 | 136 | 35 | 0.014 | 463 | 47 | 23.5 | |
| | 40 | 228 | 58.5 | 0.016 | 446 | 72 | 36 | |
| | 50 | 332 | 85 | 0.017 | 432 | 105 | 51 | |
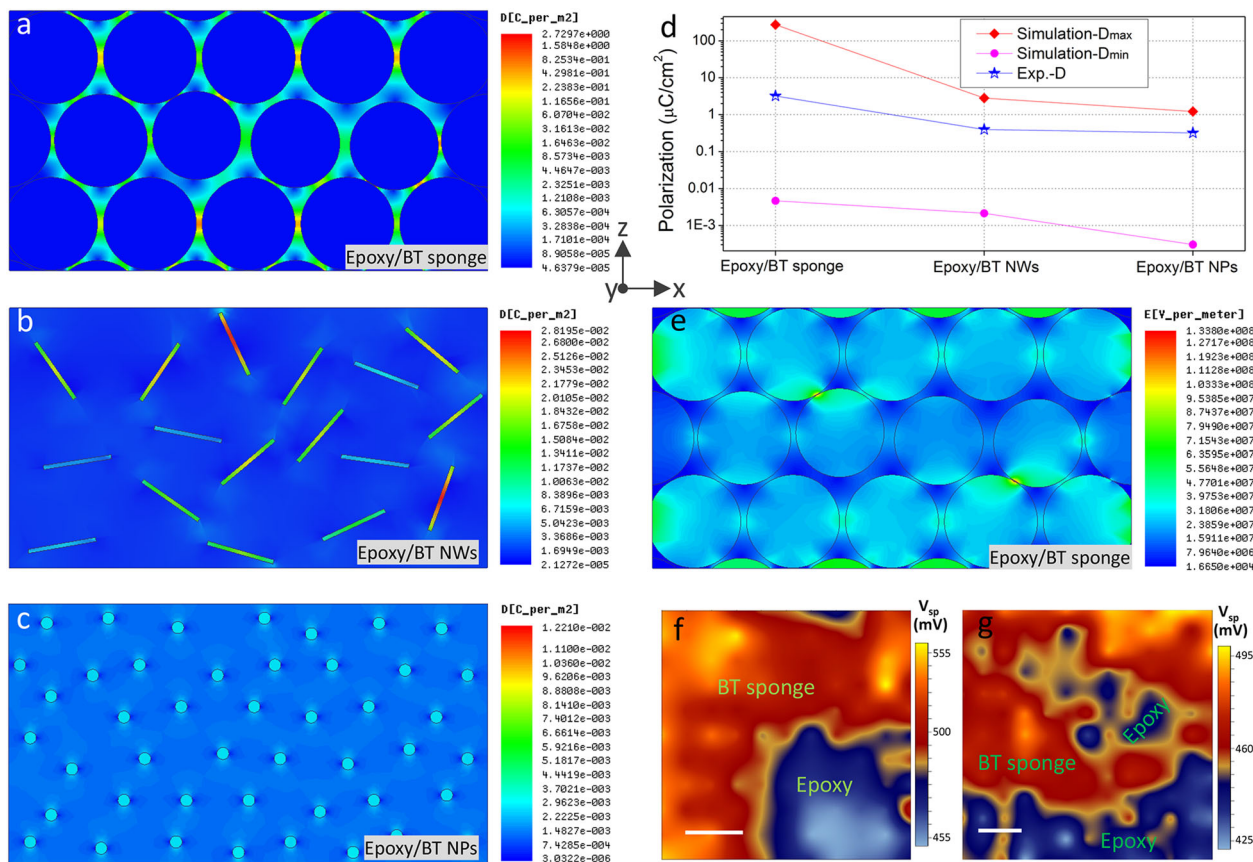
**Fig. 8 Analysis of local electric displacement in composites.** The simulated distribution by FEA of electric displacement in composites of **a** epoxy/BT sponge, **b** epoxy/BT NWs, and **c** epoxy/BT NPs. **d** Comparison of the simulated maximum (Simulation-$D_{max}$) and minimum electric displacement (Simulation-$D_{min}$) and the experimental electric displacement (Exp.$-D$) at 100 kV cm$^{-1}$ for epoxy/BT sponge, epoxy/BT NWs, and epoxy/BT NPs composites. **e** The simulated distribution by FEA of electric field in the epoxy/BT sponge composite. **f, g** Experimentally measured SKPM surface potential ($V_{sp}$) distributions of the epoxy/BT sponge composite (scale bars: 20 μm).

with different BT architectures, which can be confirmed from the simulated minimum electric displacement ($D_{min}$) and the maximum electric displacement ($D_{max}$). For a fixed electric field (i.e., 100 kV cm$^{-1}$), the simulated $D_{min}$ are ~4.64 × 10$^{-5}$, ~2.13 × 10$^{-5}$, and ~0.3 × 10$^{-5}$ μC cm$^{-2}$; and the simulated $D_{max}$ are ~272.97, ~2.82, and ~1.22 μC cm$^{-2}$ for epoxy/BT sponge, epoxy/BT NWs, and epoxy/BT NPs composites, respectively. Macroscopic $D$ is the sum of the electric moment ($D_i$) in a unit volume ($V$), $D = \sum D_i / V$[54], thus, it can be deduced that $D$ in the epoxy/BT sponge composite is greatly higher than that in epoxy/BT NWs and BT/NPs composites, which is also consistent with experimental results (Fig. 8d). It is also found that the high-electric displacement locally falls in parts of the BT sponge, while the low-electric displacement falls in the epoxy. Therefore, the enhanced electric displacement in epoxy/BT composites can be explained by the ultra-high local polarizations. $D_i$ consists of the intrinsic electric moment ($p_0$) and contribution from effective electric field ($E_e$) and the polarizability ($\alpha$), i.e., $D_i = p_0 + \alpha E_e$. $E_e$ consists of the hollow sphere electric field ($G$) and the reaction electric field ($R$). The expression of $D_i$ as a function of the external electric field ($E$) is expressed as[55,56]

$$D_i = p_0 + \frac{3\varepsilon\alpha}{2\varepsilon + 1}E + \frac{2N(\varepsilon - 1)}{3\varepsilon_0(2\varepsilon + 1)}D_i \qquad (5)$$

where $\varepsilon$ is the dielectric constant for the particle, $N$ is the number of particles per unit volume. In Eq. (5), $D_i$ increases with the polarizability, the external electric field and $N$. Investigating a BT sponge structure, $N$ is much higher than that of BT NWs and BT

NPs-based composites due to the interconnected structure, which contributes to obtaining an increased local polarization. Figure 8e shows the simulated electric field distribution in epoxy/BT sponge composites. High electric field zones are isolated inside the material, preventing the growth of electrical trees and possessing high breakdown strengths and resultant high-energy densities[57].

Figure 8f, g show experimentally measured scanning Kelvin probe microscope (SKPM) surface potential disbributions of the epoxy/BT sponge composite. Evident surface potentials are observed between the region of the BT sponge and region of the epoxy, from which the structure of the epoxy/BT sponge also can be identified. In fact, the surface potential in the the region of the BT sponge is ~70 to ~100 mV higher than that in regions of the epoxy. This indicates that upon the scanning of the probe with an applied electric field between the bottom sample electrode and the probe[8], surface potential differences are achieved which is believed to be closely related to the unique epoxy/BT sponge architecture. Furthermore, the charge density $\sigma$ (unit: C m$^{-2}$) can be obtained from the SKPM surface potentials employing a following equation[58,59]:

$$\sigma = \varepsilon_0 \frac{\varepsilon_*}{h_*} V_{sp} \qquad (6)$$

where $\varepsilon_*$ is the dielectric constant of the sample in the detected area, $h_*$ is the thickness of the sample, $V_{sp}$ is the SKPM surface potential. According to Eq. (6), surface charge densities increase with the dielectric constant of the material and the surface potentials. Because of the much larger dielectric constant of BT

(3000) than that of the epoxy (3.9) and the surface potential distribution on the two materials in composites, the induced charge density (unit: $\mathrm{C\,m^{-2}}$), i.e., the electric displacement (unit: $\mathrm{\mu C\,cm^{-2}}$) under a fixed electric field is much higher in BT sponge structures than that in the epoxy, which also can apply to spatial BT sponge structure in the three-dimensional composite. The SKPM result is consistent with simulation about the high local electric displacement in the epoxy/BT sponge composites.

**Conclusion**. We present a strategy of design of polymer composites filled with porosity tunable three-dimensional BT sponge having high dielectric constants and energy densities for energy storage. An annular interconnected BT architecture is formed which filled epoxy composites exhibit a greatly enhanced dielectric constant of $\varepsilon_r \sim 332$ at 1 kHz compared with the value of the neat epoxy and epoxy composites filled with BT NPs and BT NWs, a high $\varepsilon_r/\varepsilon_m$ and low tan$\delta$. Dielectric constants of BT sponges, BT NWs, and BT NPs-based epoxy composites fit the EMT model with determined values[21], revealing filler architectures' great influence on dielectric constants of composites.

The epoxy/BT sponge composites not only exhibit excellent dielectric performances, but also exhibit superior energy storage properties. The annular interconnected BT architecture has tilted the electric field distribution from the FEA investigations, which leads to high breakdown strength in the composite compared with those filled with vertically aligned BT fillers. High electric displacement ($3.2\,\mathrm{\mu C\,cm^{-2}}$ at $100\,\mathrm{kV\,cm^{-1}}$, $13.2\,\mathrm{\mu C\,cm^{-2}}$ at $400\,\mathrm{kV\,cm^{-1}}$) and resultant high-energy density ($105\times10^{-3}\,\mathrm{J\,cm^{-3}}$ at $100\,\mathrm{kV\,cm^{-1}}$, $1812\times10^{-3}\,\mathrm{J\,cm^{-3}}$ at $400\,\mathrm{kV\,cm^{-1}}$) and high efficiencies are achived in the epoxy/BT sponge composites, which are significantly enhanced compared with polymer/ceramic composites made from traditional strategies[16,45,50–52]. Simulation as well as SKPM results show that enhancements of electric displacements and energy densities are mainly owing to the high local electric displacement. This study demonstrates a strategy of obtaining large dielectric constants and energy densities in polymer/ceramic composites for energy storage device applications.

## Methods
**Preparation of BT sponges**. BT NPs with a mean diameter of ~40 nm were synthesized by sol–gel method: 0.1 mol of barium acetate (99%, Aladdin, China) was dissolved into 66.7 mL of deionized water while 0.1 mol of titanate butoxide (98%, Aladdin, China) was dissolved into ethanol/acetic acid mixture (3:1 in volume), respectively. The Ba solution was added into Ti solution under stirring for 10 min, after continuous stirring of the solution for 12 h, the sol–gel transition occurs. Dried the BT gel and calcined it at 700 °C for 2 h in air, BT NPs were obtained.

BT sponges with tunable porosity were fabricated by introducing PMMA microspheres (~50 μm in diameter, Mitsubishi, Japan) as the pore-generating agent. The pre-synthesized BT NPs were mixed completely with PMMA microspheres to form powder mixtures. The volume fraction of PMMA, $f_{\mathrm{PMMA}} = V_{\mathrm{PMMA}}/(V_{\mathrm{PMMA}} + V_{\mathrm{BT}})$ is in the range of 50–80 vol%, where $V_{\mathrm{PMMA}}$ and $V_{\mathrm{BT}}$ are volumes of PMMA and BT particles, respectively. Polyvinyl alcohol (PVA, Aladdin, China) solution (5 wt%) acting as a binder was added to the mixed powders, then powders were compressed into cylindrical pellets at 12 MPa for 15 s. The pellets were first calcined at 450 °C for 2 h in air to decompose the PMMA and to generate in situ pores, and then sintered at 1250 °C for 6 h in air to have free-standing BT sponge structures.

**Preparation of epoxy/BT sponge composites**. The A–B two-component liquid epoxy (315AB) with relatively low viscosities (A component, ~210 mPa s at 25 °C; B component, ~30 mPa s at 25 °C) was purchased from YaSong Adhesive Co., China. The A and B components of the liquid epoxy (3:1 in weight) were mixed and stirred for 15 min, followed by immersing the BT sponges into the solution for 2 h, and then vacuum de-foamed at ~–0.1 MPa for 30 min to completely discharge air bubbles. Subsequently, the mixture was cured at room temperature for 36 h to obtain composites and cut into specific sizes and surface-polished. For comparison, the neat epoxy and epoxy composites filled with BT NPs (~40 nm, pre-synthesized by sol–gel) and BT NWs (~10 μm length, ~0.2 μm diameter, the preparation method is shown in Supplementary Methods) with filler loadings of 20–50 vol% (~300 μm thick) were also prepared. The epoxy and composite samples were

100–300 μm in thickness. Silver pastes were printed on surfaces of samples for measurements of electrical properties.

**XRD and FTIR spectra**. To confirm the phase, XRD patterns of BT NPs, BT sponge, and epoxy/BT sponge composites were obtained using a PANalytical B.V. diffractometer with Cu Kα radiation at the wavelength of 1.540598 Å. A scanning rate of 0.05° s$^{-1}$ and a 2$\theta$ angle range of 20–80° were adopted for XRD analyses. The FTIR analysis was conducted to confirm the composition in epoxy/BT sponge composites, which was carried out on an Agilent Cary 630 spectrometer in a wavenumber range of 500–2500 cm$^{-1}$.

**SEM characterizations**. The morphology observation of epoxy/BT sponge composites was carried out using a Hitachi SU8010 and adopting 5 kV of the acceleration voltage. EDX analyses were conducted using a Noran spectrometer on the platform of the Hitachi SU8010.

**Surface potential measurements**. The surface potential distribution of epoxy/BT sponge composites was measured by a SKPM (Princeton Applied Research, AMETEK, Inc.). The composite samples were polished to have a thickness of ~80 μm before the test which was placed on the Al substrate. The distance between the tip and the samples was 10 μm. The surface charge density distribution was calculated from results of the surface potential distribution.

**Mechanical property measurement**. It was conducted by using a CMT 5254 universal electromechanical tester. Samples were prepared based on ISO 34 and 37 for the test of mechanical properties.

**TGA measurement**. The TGA of epoxy/BT sponge composites was conducted using Netzsch STA 449F3 in air within a temperature from room temperature to 800 °C.

**Electrical property measurements**. Characterization of electrical properties was conducted for at least five capacitors on multiple samples of each filler-loading variant. Dielectric properties ($\varepsilon_r$, $\varepsilon''$, and tan$\delta$) of dielectric materials were measured using a E4980A impedance analyzer (Agilent Technologies) in a frequency range of 10 Hz–1 MHz. Breakdown tests were conducted by a Cs2674ax DC breakdown tester (Changsheng Inc.) adopting a holding time of 10 s. D–E hysteresis loops were recorded utilizing a TF analyzer 2000 tester (aixACCT Technologies) with a voltage range of 0–5000 V. The practical discharge characteristic of epoxy/BT sponge composties were measured using following procedures. The composite capacitor with a fixed capacitance of ~2 μF at 1 kHz was first charged to 100 kV cm$^{-1}$ by a DC voltage supplier. Then, the composite capacitor was discharged through a load resistor in series ($R_L$) of 2 kΩ. The voltage ($V_c$) changing of the composite capacitor was recorded by a Tektronix TBS1072B oscilloscope with an internal resistance of 100 MΩ. The practial discharge power and energy were obtained from $V_c^2/R_L$ and $\int V_c^2/R_L\,dt$, respectively, where $t$ is the discharge time. Finally, the practial discharged energy density was obtained from the discharged energy per unit volume of the composite capacitor.

**Statistical analysis**. For dielectric and energy storage analysis, at least five samples were measured for each experiment. Error bars are obtained from standard error of the mean (SEM) approach with a $p$ value of ≤0.05. For all graphical analyses, mean values and SEM values were included. For breakdown strength test, at least 10 samples were measured for each experiment; a Weibull distribution was employed to analyze the data.

## Data availability
The data supporting the plots and findings in this paper is available from the corresponding author upon reasonable request.

## Code availability
ANSYS code for the simulation of the electrical properties in epoxy/BT sponge composites in Fig. 8a–e is available from the corresponding author upon reasonable request.

## References
1.  Rao, Y. & Wong, C. P. Material characterization of a high-dielectric-constant polymer–ceramic composite for embedded capacitor for RF applications. *J. Appl. Polymer Sci.* **92**, 2228–2231 (2004).

2. Li, Q. et al. Flexible high-temperature dielectric materials from polymer nanocomposites. *Nature* **523**, 576 (2015).

3. Liang, X. et al. $BaTiO_3$ internally decorated hollow porous carbon hybrids as fillers enhancing dielectric and energy storage performance of sandwich-structured polymer composite. *Nano Energy* **68**, 104351 (2020).

4. Palneedi, H., Peddigari, M., Hwang, G. T., Jeong, D. Y. & Ryu, J. High-performance dielectric ceramic films for energy storage capacitors: progress and outlook. *Adv. Funct. Mater.* **28**, 1803665 (2018).

5. Li, J., Zhang, L. & Ducharme, S. Electric energy density of dielectric nanocomposites. *Appl. Phys. Lett.* **90**, 132901 (2007).

6. Chu, B. et al. A dielectric polymer with high electric energy density and fast discharge speed. *Science* **313**, 334–336 (2006).

7. Luo, H. et al. Interface design for high energy density polymer nanocomposites. *Chem. Soc. Rev.* **48**, 4424–4465 (2019).

8. Arbatti, M., Shan, X. & Cheng, Z. Y. Ceramic–polymer composites with high dielectric constant. *Adv. Mater.* **19**, 1369–−1372 (2007).

9. Rao, Y., Ogitani, S., Kohl, P. & Wong, C. P. Novel polymer–ceramic nanocomposite based on high dielectric constant epoxy formula for embedded capacitor application. *J. Appl. Polym. Sci.* **83**, 1084–1090 (2012).

10. Avila, H. A. et al. Dielectric behavior of epoxy/$BaTiO_3$ composites using nanostructured ceramic fibers obtained by electrospinning. *ACS Appl. Mater. Interfaces* **5**, 505–510 (2013).

11. Tang, H., Malakooti, M. H. & Sodano, H. A. Relationship between orientation factor of lead zirconate titanate nanowires and dielectric permittivity of nanocomposites. *Appl. Phys. Lett.* **103**, 222901 (2013).

12. Wang, G., Deng, Y., Xiang, Y. & Guo, L. Fabrication of radial ZnO nanowire clusters and radial ZnO/PVDF composites with enhanced dielectric properties. *Adv. Funct. Mater.* **18**, 2584–2592 (2008).

13. Pan, Z., Yao, L., Ge, G., Shen, B. & Zhai, J. High-performance capacitors based on $NaNbO_3$ nanowires/poly(vinylidene fluoride) nanocomposites. *J. Mater. Chem. A* **6**, 14614–14622 (2018).

14. Xie, B. et al. Enhanced energy density of polymer nanocomposites at a low electric field through aligned $BaTiO_3$ nanowires. *J. Mater. Chem. A* **5**, 6070–6078 (2017).

15. Tang, H., Lin, Y. & Sodano, H. A. Enhanced energy storage in nanocomposite capacitors through aligned PZT nanowires by uniaxial strain assembly. *Adv. Energy Mater.* **2**, 469–476 (2012).

16. Luo, S. et al. Construction of a 3D-$BaTiO_3$ network leading to significantly enhanced dielectric permittivity and energy storage density of polymer composites. *Energy Environ. Sci.* **10**, 137–144 (2017).

17. Zhang, G. et al. Flexible three-dimensional interconnected piezoelectric ceramic foam based composites for highly efficient concurrent mechanical and thermal energy harvesting. *Energy Environ. Sci.* **11**, 2046–2056 (2018).

18. Zheng, L., Liang, G., Gu, A., Yuan, L. & Guan, Q. Unique pure barium titanate foams with three-dimensional interconnecting pore channels and their high-$k$ cyanate ester resin composites at very low barium titanate loading. *J. Mater. Chem C* **4**, 10654–10663 (2016).

19. Wucherer, L., Nino, J. C. & Subhash, G. Mechanical properties of $BaTiO_3$ open-porosity foams. *J. Eur. Ceram. Soc.* **29**, 1987–1993 (2009).

20. Wucherer, L., Nino, J. C., Basoli, F. & Traversa, E. Synthesis and characterization of $BaTiO_3$-based foams with a controlled microstructure. *Int. J. Appl. Ceram. Technol.* **6**, 651–660 (2009).

21. Rao, Y., Qu, J., Marinis, T. & Wong, C. P. A precise numerical prediction of effective dielectric constant for polymer–ceramic composite based on effective-medium theory. *IEEE Trans. Compon. Packag. Technol.* **23**, 680–683 (2000).

22. Ramesh, S., Leen, K. H., Kumutha, K. & Arof, A. K. FTIR studies of PVC/PMMA blend based polymer electrolytes. *Spectrochim. Acta A* **66**, 1237–1242 (2007).

23. Wang, P., Fan, C., Wang, Y., Ding, G. & Yuan, A. dual chelating sol–gel synthesis of $BaTiO_3$ nanoparticles with effective photocatalytic activity for removing humic acid from water. *Proc. Mater. Res. Bull.* **48**, 869–877 (2013).

24. Ni, Q. Q., Zhu, Y. F., Yu, L. J. & Fu, Y. Q. One-dimensional carbon nanotube@barium titanate@polyaniline multiheterostuctures for microwave absorbing application. *Nanoscale Res. Lett.* **10**, 174 (2015).

25. Srinivasan, M. & White, T. Degradation of methylene blue by three-dimensionally ordered macroporous titania. *Environ. Sci. Technol.* **41**, 4405–4409 (2007).

26. Dang, Z. M., Yu, Y. F., Xu, H. P. & Bai, J. Study on microstructure and dielectric property of the $BaTiO_3$/epoxy resin composites. *Comp. Sci. Technol.* **68**, 171–177 (2008).

27. Singha, S. & Thomas, M. J. Influence of filler loading on dielectric properties of epoxy–ZnO nanocomposites. *IEEE Trans. Dielectr. Electr. Insul.* **16**, 531–542 (2009).

28. Tang, H., Zhou, Z. & Sodano, H. A. Vertically aligned arrays of $BaTiO_3$ nanowires. *ACS Appl. Mater. Interfaces* **6**, 5450–5455 (2014).

29. Vijayan, P. P., Puglia, D., Kenny, J. M. & Thomas, S. Effect of organically modified nanoclay on the miscibility, rheology, morphology and properties of epoxy/carboxyl-terminated (butadiene-co-acrylonitrile) blend. *Soft Mater* **9**, 2899–2911 (2013).

30. Konnola, R. & Joseph, K. Effect of side-wall functionalisation of multi-walled carbon nanotubes on the thermo-mechanical properties of epoxy composites. *RSC Adv.* **6**, 23887–23899 (2016).

31. Jian, G. et al. Microstructure and multiferroic properties of $BaTiO_3$/$CoFe_2O_4$ films on $Al_2O_3$/Pt substrates fabricated by electrophoretic deposition. *J. Eur. Ceram. Soc.* **33**, 1155–1163 (2013).

32. Chandradass, J. & Bae, D. S. Preparation and properties of barium titanate nanopowder/epoxy composites. *J. Mater. Manuf. Process.* **23**, 116–122 (2008).

33. Phan, T. T. M. et al. The role of epoxy matrix occlusions within $BaTiO_3$ nanoparticles on the dielectric properties of functionalized $BaTiO_3$/epoxy nanocomposites. *Composite Part A* **90**, 528–535 (2016).

34. Perrier, G. & Bergeret, A. Maxwell–Wagner–Sillars relaxations in polystyrene–glass–bead composites. *J. Appl. Phys.* **77**, 2651–2658 (1995).

35. Huang, X. et al. Role of interface in highly filled epoxy/$BaTiO_3$ nanocomposites. Part I—correlation between nanoparticle surface chemistry and nanocomposite dielectric property. *IEEE Trans. Dielect. Electr. Insul.* **21**, 467–479 (2014).

36. Wu, Y., Zhao, X., Li, F. & Fan, Z. J. Evaluation of mixing rules for dielectric constants of composite dielectrics by MC-FEM calculation on 3D cubic lattice. *J. Electroceram.* **11**, 227–239 (2003).

37. Zakri, T., Laurent, J. P. & Vauclin, M. Theoretical evidence for 'Lichtenecker's mixture formulae' based on the effective medium theory. *J. Phys. D* **31**, 1589–1594 (1998).

38. Simpkin, R. Derivation of Lichtenecker's logarithmic mixture formula from Maxwell's equations. *IEEE Trans. Microw. Theory Tech.* **58**, 545–550 (2010).

39. Dang, Z. et al. Fundamentals, processes and applications of high-permittivity polymer–matrix composites. *Prog. Mater. Sci.* **57**, 660–723 (2012).

40. Yu, X., Yan, H., Zhang, G. & Wang, H. *Simulation and Design of Printed Circuit Boards Utilizing Novel Embedded Capacitance Material*, 2 (IEEE, Huawei Technologies Co., Ltd, Pudong ShangHai, China, 2010).

41. Arva, M. C. & Diaconescu, E. Modeling of stackable embedded capacitors into the PCB layers. In *Proc. 11th International Conference on Technical and Physical Problem of Electrical Engineering*, Bucharest, 10–12 (ICTPE Conference, 2015).

42. Huang, X. et al. Role of interface in highly filled epoxy/$BaTiO_3$ nanocomposites. part II—effect of nanoparticle surface chemistry on processing, thermal expansion, energy storage and breakdown strength of the nanocomposites. *IEEE Trans. Dielectr. Electr. Insul.* **21**, 480–487 (2014).

43. Cho, S. D., Lee, S. Y., Hyun, J. G. & Paik, K. W. Comparison of theoretical predictions and experimental values of the dielectric constant of epoxy/$BaTiO_3$ composite embedded capacitor films. *J. Mater. Sci. Mater. Electron.* **16**, 77–84 (2015).

44. Xu, J., Bhattacharya, S., Pramanik, P. & Wong, C. P. High dielectric constant polymer–ceramic (epoxy varnish-barium titanate) nanocomposites at moderate filler loadings for embedded capacitors. *J. Electron. Mater.* **35**, 2009–2015 (2006).

45. Fu, J. et al. Improving dielectric properties of PVDF composites by employing surface modified strong polarized $BaTiO_3$ particles derived by molten salt method. *ACS Appl. Mater. Interfaces* **7**, 24480–24491 (2015).

46. Jian, G. et al. A strategy for design of non-percolative composites with stable giant dielectric constants and high energy densities. *Nano Energy* **58**, 419–426 (2019).

47. Fillery, S. P. et al. Nanolaminates: increasing dielectric breakdown strength of composites. *ACS Appl. Mater. Interfaces* **3**, 1388–1396 (2012).

48. Zhang, X., He, Q., Gu, H., Wei, S. & Guo, Z. Polyaniline stabilized barium titanate nanoparticles reinforced epoxy nanocomposites with high dielectric permittivity and reduced flammability. *J. Mater. Chem. C* **1**, 2886–2899 (2013).

49. Gorzkowski, E. P. & Pan, M. J. Barium titanate-polymer composites produced via directional freezing. *IEEE Trans. Ultrason. Ferroelectr. Freq. Control* **56**, 1613–1616 (2009).

50. Manika, G. C. & Psarras, G. C. Energy storage and harvesting in $BaTiO_3$/epoxy nanodielectrics. *High Voltage* **1**, 151–157 (2016).

51. Tomer, V., Polizos, G., Manias, E. & Randall, C. A. Epoxy-based nanocomposites for electrical energy storage. I: effects of montmorillonite and barium titanate nanofillers. *J. Appl. Phys.* **108**, 074116 (2010).

52. Polizos, G., Tomer, V., Manias, E. & Randall, C. A. Epoxy-based nanocomposites for electrical energy storage. II: Nanocomposites with nanofillers of reactive montmorillonite covalently-bonded with barium titanate. *J. Appl. Phys.* **108**, 074117 (2010).

53. Tang, H. & Sodano, H. A. Ultra high energy density nanocomposite capacitors with fast discharge using $Ba_{0.2}Sr_{0.8}TiO_3$ nanowires. *Nano Lett.* **13**, 1373–1379 (2013).

54. Prateek, V. K. T. & Gupta, R. K. Recent progress on ferroelectric polymer-based nanocomposites for high energy density capacitors: synthesis, dielectric properties, and future aspects. *Chem. Rev.* **116**, 4260–4317 (2016).

55. Onsager, L. Electric moments of molecules in liquids. *J. Am. Chem. Soc.* **58**, 1486–1493 (1936).

56. Block, H. & Walker, S. M. A modification of the onsager theory for a dielectric. *Chem. Phys. Lett.* **19**, 363–364 (1973).
57. Guo, R. et al. Significantly enhanced permittivity and energy density in dielectric composites with aligned $BaTiO_3$ lamellar structures. *J. Mater. Chem. A* **8**, 3135–3144 (2020).
58. Melitz, W., Shen, J., Kummel, A. C. & Lee, S. Kelvin probe force microscopy and its application. *Surf. Sci. Rep.* **66**, 1–27 (2011).
59. Liu, J., Gaikwad, R., Hande, A., Das, S. & Thundat, T. Mapping and quantifying surface charges on clay nanoparticles. *Langmuir* **31**, 10469–10476 (2015).

## Acknowledgements

## Author contributions

G.J., Z.W., C.Y., and C.-P.W. conceived the basic idea and designed experiments. Y.J. synthesized BT sponge structures and prepared epoxy composites. Y.J. and Q.M. conducted microstructure characterizations. G.J. and Y.J. investigated dielectric, insulating, and energy storage properties of composites. Y.J. conducted the finite-element simulation. G.J., Y.J., J.Z., C.Y., K.-S.M., and C.-P.W. analyzed the experimental data. G.J. and K.-S.M. wrote the manuscript and prepared the supplementary data.

## Competing interests

The authors declare no competing interests.

## Additional information

**Supplementary information** is available for this paper at https://doi.org/10.1038/s43246-020-00092-0.

**Correspondence** and requests for materials should be addressed to G.J. or C.-P.W.

**Reprints and permission information** is available at http://www.nature.com/reprints

**Publisher's note** Springer Nature remains neutral with regard to jurisdictional claims in published maps and institutional affiliations.